10-17-2017

Capturing species-level drought responses in a temperate deciduous forest using ratios of photochemical reflectance indices between sunlit and shaded canopies

Taehee Hwang

Hamed Gholizadeh

Daniel A. Sims

Kimberly A. Novick

Edward R. Brzostek

See next page for additional authors

Authors

Taehee Hwang, Hamed Gholizadeh, Daniel A. Sims, Kimberly A. Novick, Edward R. Brzostek, Richard P. Phillips, Daniel T. Roman, Scott M. Robeson, and Abdullah F. Rahman

Capturing species-level drought responses in a temperate deciduous forest using ratios of photochemical reflectance indices between sunlit and shaded canopies

Taehee Hwang[1,§,*], Hamed Gholizadeh[1,§], Daniel A. Sims[1,§], Kimberly A. Novick[2], Edward R. Brzostek[3,4], Richard P. Phillips[4], Daniel T. Roman[2,5], Scott M. Robeson[1], Abdullah F. Rahman[1,6]

[1]Department of Geography, Indiana University Bloomington, Bloomington, IN 47401, USA
[2]School of Public and Environmental Affairs, Indiana University Bloomington, Bloomington, IN 47401, USA
[3]Department of Biology, Indiana University Bloomington, Bloomington, IN 47401, USA
[4]Department of Biology, West Virginia University, Morgantown, WV 26506, USA
[5]U.S. Department of Agriculture, Forest Service, Northern Research Station, Grand Rapids, MN, 55744, USA
[6]Coastal Studies Lab, University of Texas Rio Grande Valley, South Padre Island, TX, 78597, USA

[*]Corresponding author: Taehee Hwang
Email: taehee@indiana.edu
Tel: (812) 856-2846

[§]These three authors equally contributed to the paper

Submitted to Remote Sensing of Environment

Abstract

To classify trees along a spectrum of isohydric to anisohydric behavior is a promising new framework for identifying tree species' sensitivities to drought stress, directly related to the vulnerability of carbon uptake of terrestrial ecosystems with increased hydroclimate variability. Trees with isohydric strategies regulate stomatal conductance to maintain stationary leaf water potential, while trees with anisohydric strategies allow leaf water potential to fall, which in the absence of significant hydraulic cavitation, will facilitate greater rates of carbon uptake. Despite the recognition of the gas exchange consequences of isohydric and anisohydric strategies for individual tree species, there have been few studies regarding whether isohydric trees produces distinct spectral signatures under drought stress that can be remotely sensed. Here, we examined the capability of four vegetation indices (PRI, NDVI, $NDVI_{705}$, and EVI) to capture the differences in spectral responses between isohydric and anisohydric trees within a deciduous forest in central Indiana, USA. Both leaf-level spectral measurements and canopy-scale satellite observations were used to compare peak growing-season spectral signatures between a drought and a non-drought year. At the leaf scale, two vegetation indices (NDVI and $NDVI_{705}$) failed to capture the drought signal or the divergent isohydric/anisohydric behavior. EVI successfully captured the drought signal at both leaf and canopy scales, but failed to capture the divergent behavior between isohydric and anisohydric tree species during the drought. PRI captured both drought signals and divergent isohydric/anisohydric behavior at both leaf and canopy scales once normalized between sunlit (backward direction images) and shaded (forward direction images) portions of canopy, which indicates drought stress and subsequent photosynthetic downregulation are greater in the sunlit portion of canopy. This study presents a significant step forward in our ability to directly mapping emergent isohydricity at different scales based on divergent spectral signatures between sunlit and shaded canopies.

Keywords: PRI, isohydricity, drought, LUE, imaging spectroscopy, MODIS

Introduction

Recently, many forested regions in the United States have experienced increasing drought stress under ongoing climate change (Dai 2013). Warmer temperatures have increased hydroclimate variability (Seager *et al.*, 2009; O'Gorman and Schneider, 2009) with more frequent droughts, contributing to acute reductions in net ecosystem productivity (Roman et al. 2015), prolonged water stress (Brzostek et al. 2014; Xu and Baldocchi 2003), and widespread tree mortality (Adams et al. 2009; Allen and Breshears 2007; McDowell and Allen 2015) in forested ecosystems. Differences between tree species in their response to imposed hydrologic stress can be evaluated by characterizing species along a continuum of isohydric to anisohydric behavior (Choat et al. 2012; Klein et al. 2014; Martinez-Vilalta et al. 2014). Despite the risk of xylem cavitation associated with highly negative leaf water potentials, trees with anisohydric strategies frequently sustain high stomatal conductance during drought (Matheny et al. 2016; Meinzer et al. 2017; Roman et al. 2015; Yi et al. 2017). In the absence of significant xylem cavitation, this strategy can also support relatively high levels of photosynthesis during periods of drought stress. In contrast, trees with isohydric strategies regulate stomatal conductance to maintain a relatively stationary leaf water potential as soil moisture declines. This strategy reduces embolism risk, but at a cost of reduced carbon assimilation (McDowell et al. 2008). The ratio of drought-driven declines in carbon uptake as compared to stomatal conductance depends on the plasticity of the plant's intrinsic water use efficiency, which can increase during periods of hydraulic stress, but not typically to an extent to completely mitigate losses in carbon uptake linked to stomatal closure (Novick et al. 2015). In relatively mesic forests like Eastern US, where drought events can have large effects on carbon and water cycling but rarely cause extensive hydraulic failure, the isohydric/anisohydric continuum is well suited for predicting the extent to which trees regulate their stomates during drought periods (Novick et al. 2015; Roman et al. 2015; Yi et al. 2017), as well as the resulting carbon assimilation strategies. The sensitivity of gross primary production (GPP) to drought stress has been shown to depends strongly on the relative proportion of isohydric vs.

78 anisohydric tree species in forest stands (Roman et al. 2015). Recent works also suggest that isohydric
79 stands are associated with greater interannual variability of evapotranspiration and reduced
80 productivity compared to anisohydric stands, as related to strong isohydric behavior in their stomatal
81 control and cavitation vulnerability (Ford et al. 2011; Novick et al. 2016; Stoy et al. 2006). As a result,
82 the degree to which forest stands respond isohydrically or anisohydrically to drought stress directly
83 influences ecosystem productivity and has the potential to cause cascading effects on regional carbon
84 storage.
85 While diagnosing isohydric vs. anisohydric stomatal responses is relatively straightforward, albeit
86 labor-intensive, at the tree level (Meinzer et al. 2016), we have little understanding of how this
87 behavior can be detected at large scales using remote sensing data. Specifically, there has been limited
88 research regarding whether isohydric and anisohydric trees possess distinct spectral responses under
89 drought stress (Sims et al. 2014) that can be remotely sensed and mapped to parameterize large-scale
90 GPP models (Konings and Gentine 2016; Sperry et al. 2016). Classically, light use efficiency (LUE)
91 based GPP models have been widely used to assess the impact of droughts on carbon sequestration at
92 a global scale (e.g. Song et al. 2013). In these models, GPP is usually proportional to the multiplicative
93 term between LUE and absorbed photosynthetically active radiation (APAR). However, remote
94 sensing metrics of canopy greenness often fail to capture small changes in leaf area or its function (i.e.
95 stomatal closure) that accompany drought (Asner et al. 2004; Hwang et al. 2008; Sims et al. 2014).
96 For this reason, most remote-sensing based terrestrial productivity models use water stress functions
97 that downregulate LUE values under conditions of low water availability, based on either vapor
98 pressure deficit (VPD) or soil moisture metrics (Song et al. 2013). These models are often applied to a
99 wide range of vegetation composition and formulate the stomatal responses with a single set of
100 ecophysiological model parameters based on the major plant functional types (e.g. Biome Parameter
101 Look-Up Table for MODIS GPP; Zhao et al. 2005). Consequently, current model structures cannot
102 reproduce observed differences in drought sensitivity among isohydric and anisohydric species within

103 temperate deciduous forests. This mismatch between our theoretical understanding of plant drought
104 response and its representation in models highlights a critical knowledge gap in understanding the
105 vulnerability of carbon sequestration of terrestrial ecosystems under increased hydroclimate variability,
106 especially in terms of species-specific variability with different water use and carbon assimilation
107 strategies under drought conditions.

108 Recently, there have been advances in directly mapping LUE using imaging spectroscopy from
109 different platforms. LUE mapping using remote sensing data is mostly based on the detection of
110 excess energy not used in photosynthesis especially under drought conditions (Coops et al. 2010;
111 Demmig-Adams and Adams III 1996), using the photochemical reflectance index (PRI) (Gamon et al.
112 1992; Gamon et al. 1997; Penuelas et al. 1995). PRI has been successfully applied across various
113 remote sensing platforms ranging from narrow bandwidth spectro-radiometers to the Moderate
114 Resolution Imaging Spectroradiometer (MODIS) (Drolet et al. 2008; Drolet et al. 2005; Goerner et al.
115 2009). Although PRI values are closely related to photosynthetic LUE values across different scales
116 (see Garbulsky et al. 2011), PRI-LUE relationships often show strong sensitivity to shadow fractions
117 following sun-target-sensor geometry (Drolet et al. 2005; Hall et al. 2008; Hilker et al. 2008), as well
118 as canopy structures and soil background reflectance (Barton and North 2001; Suárez et al. 2008).
119 Across forest ecosystems, the correlation between LUE and PRI for sunlit canopy is higher than
120 shaded canopy during water-stress conditions (Hall et al. 2008; Zhang et al. 2016). Expanding on this
121 framework, known correlations between view angle and canopy LUE suggest that the variability in
122 PRI values with view angle is directly related to the degree of down-regulation between sunlit and
123 shaded portions of the canopy (Coops et al. 2010; Drolet et al. 2005). Using multi-angle satellite
124 systems, such as backward and forward direction images, to capture the sunlit and shaded portion of
125 canopy, respectively (Hall et al. 2012; Hall et al. 2008), it may be possible to derive canopy responses
126 to drought (i.e. isohydry vs. anisohydry) by quantifying the extent to which sunlit and shaded canopies
127 differ in PRI.

In this paper, we hypothesize that the degree to which canopies downregulate photosynthesis under drought stress (isohydry vs. anisohydry) is directly correlated with the magnitude of the differences in PRI between sunlit and shaded portions of canopy (Coops et al. 2010). Further, using both leaf and canopy scale measurements, we seek (1) to capture the difference in leaf-scale spectral signatures between isohydric and anisohydric trees species under drought stress, and (2) to examine whether this behavior can be detected at the canopy scale using multi-angle MODIS images. To meet these objectives, we combined site-level spectral observations and remotely sensed data for a biologically diverse temperature deciduous forest that contains a broad spectrum of isohydric and anisohydric species, and that experienced an exceptionally severe drought in 2012 (Roman et al. 2015).

Methods and materials

Study area

The study site is located in the Morgan Monroe State Forest (MMSF; 39.3232°N, 86.4131°W) in central Indiana, USA. MMSF is a deciduous broadleaf forest with average canopy height and rooting depth of 27 m and 0.44 m, respectively (Ehman et al. 2002). Among the common tree species found in the study region, sugar maple (*Acer saccharum*), tulip poplar (*Liriodendron tulipifera*) and sassafras (*Sassafras albidum*) are generally recognized to be among the most isohydric (or conservative) species, whereas white and red oaks (*Quercus alba* and *Q. rubra*) are anisohydric (or non-conservative) (Choat et al. 2012; Novick et al. 2015; Roman et al. 2015). Based on measurements of trees with diameter at breast height ≥10 cm made in 54 large plots in March 2011, the study site is dominated by isohydric species such as sugar maple, tulip poplar and sassafras, which represent 21%, 25%, and 10% of total basal area, respectively, while the anisohydric white and red oaks represent 5% and 3%, respectively. The study site experienced a severe drought during the summer (June-August) of 2012. During this time period, the total rainfall was 135 mm, which is less than 50% of average June-August rainfall (302 mm from 1999-2015 except for 2012) (Figure S1; June and July rainfall was just ~10% of the

153 long-term mean). As a result, there was a dramatic early dry down of soil water content in 2012
154 (Figure 1). In field measurements and remote sensing analyses, we also include data from 2011 and
155 2013 to represent normal and wet years, respectively (Figure S1).
156

157 *Ecosystem measurements*

158 The net ecosystem exchange of CO_2 (NEE) has been continuously measured from the MMSF
159 *AmeriFlux* Tower (site code US-MMS) since 1998. Carbon dioxide and water vapor fluxes were
160 measured at the top of the tower (i.e., z = 46 m) using a sonic anemometer (CSAT-3; Campbell
161 Scientific Inc.) and a closed-path infrared gas analyzer (LI-7000; LI-COR, Lincoln, NE), which is
162 calibrated weekly. Eddy covariance NEE data were recorded continuously at a frequency of 10 Hz,
163 and filtered for periods of low turbulence (i.e. friction velocity < 0.3 m s^{-1}). Nocturnal and dormant
164 season NEE data were then used parameterize a model for ecosystem respiration (RE), which was
165 subtracted from NEE to derive an estimate of gross ecosystem productivity (GEP), as discussed in
166 detail in Dragoni et al. (2011), Schmid et al. (2000), and Sulman et al. (2016).
167 Absorbed photosynthetically active radiation (APAR) values were estimated from the difference of
168 PAR measurements between top and below the canopy. Total incoming photosynthetically active
169 radiation (IPAR) values were measured at 46-m height using a quantum sensor (BF3, Delta-T Devices
170 Ltd., Cambridge), while below-canopy PAR (PAR_{below}) values measured at 2-m height (Li-190, Li-
171 COR, Lincoln, NE). Hourly albedo (a) values were estimated from shortwave incoming and reflected
172 irradiance measurements from a net radiometer (CNR1, Kipp & Zonen, Netherlands), installed at 46-
173 m height. Hourly absorbed photosynthetically active radiation (APAR) and fraction of absorbed PAR
174 (FPAR) values were calculated as follows:

175 $$APAR = IPAR \cdot (1 - \alpha) - PAR_{below} \quad (1)$$

176 $$FPAR = APAR/IPAR \quad (2)$$

177 Hourly GEP and APAR estimates were used to calculate hourly LUE (= GEP/APAR) during the
178 peak growing season (June through August) in 2011, 2012, and 2013, each representing normal, dry,
179 and wet years, respectively. Weekly leaf area index (LAI) values have been measured along three
180 transects (n = 30 total) around the flux tower at dawn (LAI-2200, Li-COR, Lincoln, NE) during the
181 whole growing season (March-November). Volumetric soil water content (SWC) were also
182 continuously measured from the top 30 cm soil layer by reflectometer probes (CS615 and CS616;
183 Campbell Scientific, Logan, UT).
184

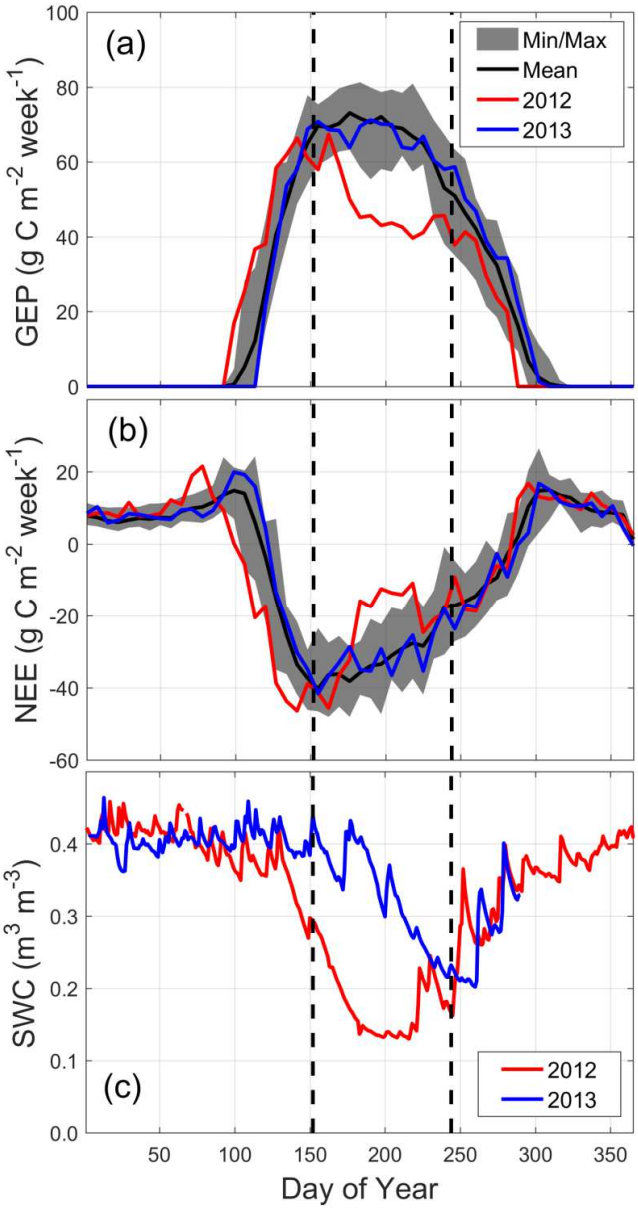

Figure 1: Long-term tower-based measurements of (a) weekly gross ecosystem productivity (GEP), (b) weekly net ecosystem exchange (NEE), and (c) mean daily volumetric soil water content (SWC) at the Morgan-Monroe State Forest flux tower in the study site. The gray regions represent the minimum and maximum ranges from 1999 to 2015, except for 2012 (drought year). The vertical dashed lines show the peak growing season (June-August). Negative NEE values represent carbon sinks.

193 *Leaf-scale spectroscopic and gas exchange measurements*

194 Using a portable field spectroradiometer (UniSpec-SC Spectral Analysis System, PP Systems Inc.,
195 Amesbury, MA) and photosynthetic system (Li-6400Xt, Li-COR, Lincoln, NE), both leaf reflectance
196 and photosynthesis were measured for the intact leaves around midday (10 am-3 pm) weekly from
197 June through August in 2012 and 2013. We selected three trees with similar sizes from each species
198 group: sugar maples (mean diameter at breast height: 44.1, 44.2, and 48.4 cm), tulip poplars (62.5,
199 62.8, and 86.7 cm), sassafras (41.4, 34.0, and 36.1 cm), and oaks (two white oaks: 39.2 and 43.8 cm,
200 one red oak: 47.6 cm). Using a 25-m boom lift, five sunlit and five shaded leaves were selected for
201 each tree from the top and bottom of the canopy, respectively. Both spectroscopic and gas exchange
202 measurements were performed on the same leaves attached to the trees, but we did not measure the
203 same leaves over the entire experiment. Leaf gas exchange measurement was performed over a short
204 period of time (less than 2 min) with chamber conditions (CO_2 concentration, temperature, humidity,
205 and PAR) set to match ambient values (Roman et al. 2015). Previous analysis of the dynamics of leaf
206 water potential (pre-dawn and midday), also collected concurrently with the gas exchange
207 measurements, have been used to show that oaks behaved very anisohydrically during the 2012
208 drought, while other species were more isohydric (Roman et al. 2015). Leaf reflectance values were
209 also measured at 3-nm intervals within the visible and near infrared electromagnetic spectrum (400-
210 1000 nm), later interpolated to 1-nm intervals. All spectral and photosynthetic measurements were
211 averaged separately for sunlit and shaded leaves of each tree. These concurrent measurements of leaf
212 reflectance and photosynthesis provide a unique opportunity to test the ability to capture isohydric vs.
213 anisohydric behavior during the severe drought using remote sensing data.
214

215 *Leaf-scale spectral indices*

216 In this study, we used four spectral indices based on narrow bands of the electromagnetic spectrum:

photochemical reflectance index (PRI), normalized difference vegetation index (NDVI), red edge NDVI ($NDVI_{705}$), and enhanced vegetation index (EVI) at both leaf- and canopy-scale spectral measurements (Table 1). PRI directly quantifies the reflectance change associated with xanthophyll absorption (at 531 nm) (Penuelas et al. 1995) and the associated LUE response (Drolet et al. 2008; Drolet et al. 2005; Garbulsky et al. 2013; Rahman et al. 2004; Zhang et al. 2016). A simple transformation was applied to PRI values to avoid negative or near-zero values, known as scaled-PRI (sPRI; Table 1). For NDVI and EVI calculations, we used the reflectance of 645, 858.5, and 469 nm wavelengths, the middle of the MODIS band 1 (red), 2 (near infrared), and 3 (blue) to facilitate the comparison with MODIS vegetation indices. The red edge NDVI ($NDVI_{705}$) represents the normalized difference between the 705 and 750 nm wavelengths, developed based on the chlorophyll index (Sims and Gamon 2002). While PRI captures drought-induced instantaneous physiological changes in the xanthophyll cycle, other leaf-scale indices were sensitive to chlorophyll-related changes during droughts (Marchin et al. 2010; Munne-Bosch et al. 2001). Additionally, the canopy-scale NDVI and EVI values also capture structural changes (e.g. LAI, leaf inclination angle etc.) accompanying droughts. We compared these four spectral indices and photosynthesis measurements during the peak drought period (July to August) in 2012 with the same period in a following wet year (2013). We examined the differences in the spectral indices in regards to the photosynthesis between dry and wet years, and between isohydric and anisohydric species both at the leaf and canopy scales. To capture the divergence in spectral indices between sunlit and shaded portions of canopy, we calculated the sunlit-to-shaded ratios in this study, such as $PRI_{sunlit}/PRI_{shaded}$. These ratio indices also make it possible to normalize seasonal changes of PRI, driven by the changes in leaf color and carotenoids-to-chlorophyll contents (Filella et al. 2009; Gamon et al. 2016; Wong and Gamon 2015).

240 Table 1: Four narrow-band spectral indices (PRI, NDVI, $NDVI_{705}$, and EVI) used in this study.

Spectral index	Equation	Reference
PRI or sPRI	$PRI = \frac{\rho_{531} - \rho_{570}}{\rho_{531} + \rho_{570}}$; $sPRI = \frac{PRI + 1}{2}$	Gamon et al. (1992), Penuelas et al. (1995) Rahman et al. (2004)
NDVI	$NDVI = \frac{\rho_{858.5} - \rho_{645}}{\rho_{858.5} + \rho_{645}}$	Tucker (1979)
$NDVI_{705}$	$NDVI_{705} = \frac{\rho_{750} - \rho_{705}}{\rho_{750} + \rho_{705}}$	Sims and Gamon (2002)
EVI	$EVI = 2.5\frac{\rho_{858.5} - \rho_{645}}{\rho_{858.5} + 6\rho_{645} - 7.5\rho_{469} + 1}$	Huete et al. (1997)

241 ρ_n is reflectance at n nm. PRI: photochemical reflectance index, NDVI: normalized difference
242 vegetation index, $NDVI_{705}$: red edge NDVI, and EVI: enhanced vegetation index
243

244 *MODIS data processing*

245 We extracted the 250-m MODIS NDVI and EVI data (MOD13Q1) around the flux tower from
246 2001 to 2014 using the MODIS Web Service Tool
247 (https://modis.ornl.gov/data/modis_webservice.html). We used only the pixel values with a 'good'
248 quality, based on the Pixel Reliability parameter (Didan and Huete 2006). The NDVI and EVI results
249 were presented by averaging a 3×2-km area around the flux tower, which represents relatively
250 homogenous forest cover. We also calculated the canopy-scale sPRI values using MODIS Terra and
251 Aqua data (collection 6) at the same spatial extent. Three MODIS products (MOD/MYD021KM,
252 MOD/MYD03, and MOD/MYD35) were downloaded from the Level-1 and Atmosphere Archive and
253 Distribution System (LAADS; https://ladsweb.nascom.nasa.gov/) for June, July, and August of 2011,
254 2012, and 2013. The MOD/MYD021KM product includes calibrated and geolocated at-aperture
255 radiances at 1-km resolution for 36 MODIS bands. We only analyzed the pixels which centroids are
256 located within the 3×2-km area in the sPRI calculation. Since the reference band used in PRI (i.e., the
257 band at 570 nm) is not available in MODIS products, we apply a modified approach proposed by
258 Drolet et al. (2005) to produce the reflectance data required to calculate sPRI.

While Drolet et al. (2005) use band 13 as the reference band, previous research at MMSF has shown that band 13 is likely saturated for terrestrial observations (Goerner et al. 2009). As a result, our calculation of PRI uses band 1 as the reference and band 11 as the detection band. Recently, this index was suggested to be renamed as a Chlorophyll/Carotenoid Index (CCI) to monitor evergreen photosynthetic activity (Gamon et al. 2016). Additionally, previous studies have shown that atmospheric correction of MODIS data does not improve the PRI results and it may even degrade the correlation between PRI and LUE (Goerner et al. 2011). So, instead of using atmospherically corrected reflectance values, we used the top-of-atmosphere (TOA) reflectance to calculate PRI (He et al. 2016). The MOD/MYD35 products were also used for cloud masking and removing cloud-covered pixels. We used only the pixels with the 'confident clear' quality flag in the MOD/MYD35 products. To remove pixels with large footprints, we eliminated all pixels with sensor zenith angle larger than 40°.

From the MODIS Terra and Aqua data, we calculated the PRI values for backward (sun is behind the sensor) and forward (sun is in front of the sensor) direction images which effectively capture the spectral signatures of sunlit and shaded portion of canopy, respectively. The solar/sensor azimuth and zenith angles and coordinates of all pixels from the MOD/MYD03 product were used to determine the backward and forward direction images. Using the solar and sensor azimuth angles obtained from MOD/MYD03 products, the relative azimuth angle Δ can be defined as follows:

$$\Delta = \begin{cases} |\theta - \theta_0| \;\; if \;\; 0° \le |\theta - \theta_0| \le 180° \\ 360° - |\theta - \theta_0| \;\; if \;\; |\theta - \theta_0| > 180°, \end{cases} \quad (3)$$

where θ and θ_0 are the sensor and solar azimuth angles, respectively. Backward direction images have a relative azimuth angle less than or equal to 60°, while forward direction images have a relative azimuth angle greater than 60° (Drolet et al. 2005). Note that the sunlit portion of canopy dominates the field of view of the sensor with smaller Δ angles (backward direction) with increasing the shaded portion with larger Δ angles (forward direction) (Cheng et al. 2012; Hall et al. 2008). In a manner similar to the leaf-scale sunlit-to-shaded sPRI ratios, the sPRI ratios were also calculated between

backward and forward direction images. However, the MODIS PRI values are not essentially paired simply because cloud-free backward and forward images were not collected on the same days, different with the tree-level measurements. To avoid no PRI values in either backward or forward direction images at a short time interval, we calculated the PRI ratios over three-week intervals during the peak growing season (June-August) from 2011 to 2013.

Statistical analyses

We performed two-sample Welch's (unequal variances) *t*-tests with a null hypothesis that the group mean of 2012 (dry year) is greater than that of 2013 (wet year) during the peak drought period (July to August). We applied this test to all four spectral indices (PRI, NDVI, $NDVI_{705}$, and EVI; Table 1) and their ratios at the tree level, as well as to all pixel-level MODIS PRI values at the canopy scale. For three groups among normal (2011), dry, (2012), and wet (2013) years, we applied the analysis of variance (ANOVA) tests to evaluate whether the means of three groups are equal.

Results

Flux and gas exchange measurements

At the canopy scale, both GEP and NEE from the flux tower were reduced to an unprecedented level during the 2012 drought event (Figure 1). During the peak drought period (July-August), the magnitudes of weekly GEP and NEE were over 30 g C m^{-2} (less than 40% of mean value) and 20 g C m^{-2} lower (less than 55% of mean value) respectively, compared to the baseline mean GEP and NEE (1999-2015 except for 2012). Significant differences in midday (10 am-3 pm) hourly APAR and GEP between 2012 and 2013 were also observed (Figure 2). Mean APAR values were significantly higher ($p < 0.01$) in 2012 (dry) than in 2013 (wet), which were largely driven by significantly higher incoming PAR due to less frequent clouds with little changes in fraction of absorbed PAR (FPAR)

(Figure S2). As a result, mean hourly LUE (=GEP/APAR) values were significantly lower in 2012 than in 2013 ($p < 0.01$). It is worthwhile to note that LUE values in the normal year (2011) were between the values in wet and dry years.

Leaf gas exchange measurements showed similar significant decreases in mean net photosynthesis (PS) during the drought ($p < 0.001$), as well as divergent behavior between isohydric and anisohydric species (Figure 3). In 2012, mean leaf PS values were reduced by about 30-50% compared to those in 2013 for the three isohydric species (sugar maple, tulip poplar, and sassafras). In the sunlit leaves, tulip poplar showed the largest percent decrease (41.6 %) in the mean values, followed by sassafras (37.7 %) and sugar maple (31.7 %). In the shaded leaves, sassafras showed the largest percent decrease (46.2 %), followed by sugar maple (40.9 %) and tulip poplar (33.8 %). Sunlit leaves usually had higher levels of PS than the shaded ones, and they showed larger decreases in the absolute magnitudes of PS during the 2012 drought. However, oaks (anisohydric) still maintained relatively high levels of PS both in sunlit and shaded leaves. While stomatal conductance of oak species was unaffected by the drought (Roman et al. 2015), there was a small (9.4 %) but significant difference ($p < 0.05$) in mean PS of sunlit oak leaves between years (Figure 3d). This could reflect non-stomatal (i.e. biochemical) limitations to the photosynthetic machinery imposed by the particularly low leaf water potential observed for these species during the drought (Roman et al. 2015). It is worthwhile to note that the decrease in PS of sunlit leaves was somewhat compensated by a significant increase in PS of shaded PS ($p < 0.05$; 21.2 %) for oak species (Figure 3d).

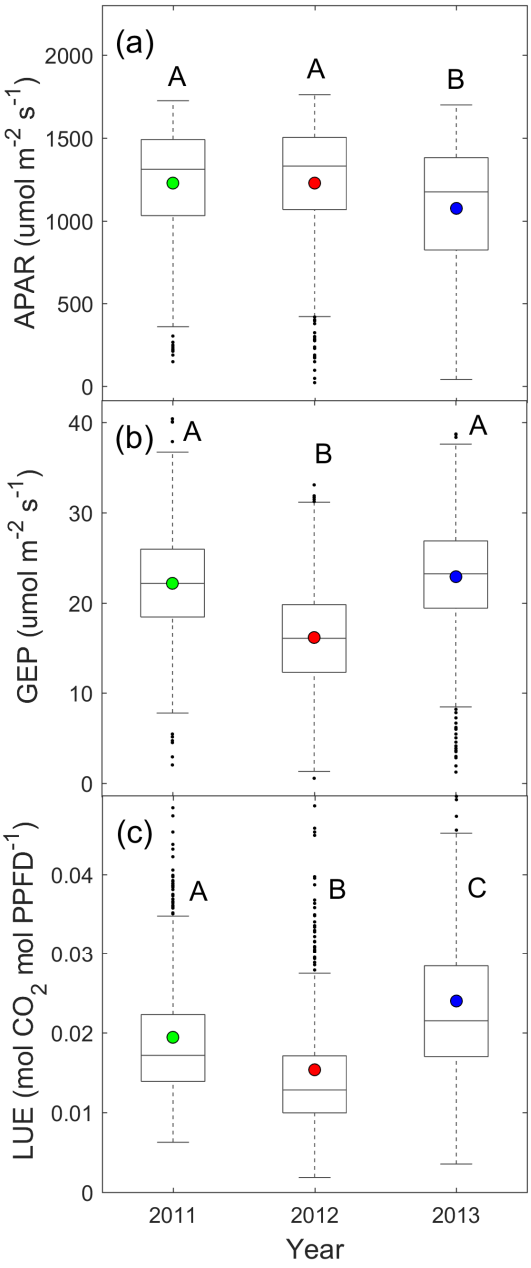

328

329 Figure 2: Hourly midday (10 am-3 pm) (a) absorbed photosynthetically active radiation
330 (APAR), (b) gross ecosystem productivity (GEP), and (c) light use efficiency (LUE) values
331 from June through August in normal (2011 – green), drought (2012 – red), and wet y(2013 –
332 blue) years from the Morgan Monroe State Forest flux tower. Circles are the mean values,
333 while black dots are outliers. Different letters (A-C) denote significant differences in the group
334 means using an analysis of variance (ANOVA) test ($p < 0.01$).

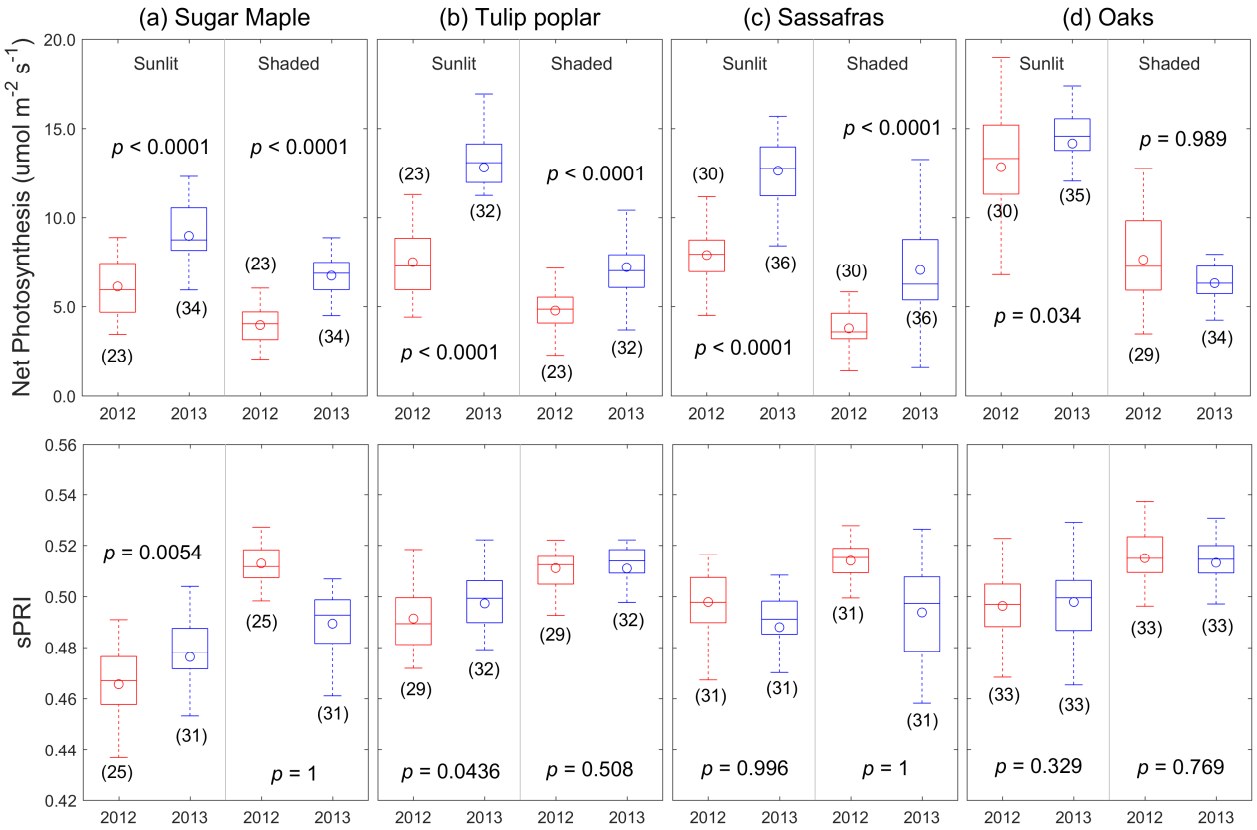

Figure 3: Boxplots for the measured leaf net photosynthesis (μmol m^{-2} s^{-1}) and sPRI values (dimensionless) from July to August in 2012 (drought year - red) and 2013 (wet year - blue) for three isohydric species: (a) sugar maple, (b) tulip poplar, (c) sassafras, and (d) two anisohydric oaks (two white oaks and one red oak). Leaf reflectance and photosynthesis were measured weekly around midday (10 am-3 pm) for sunlit and shaded leaves separately (Figure S3 and S4). All measurements represent the tree-level observations from three trees in each group (n = 12 total), which are actually the averaged values from five leaf samples from each tree. The numbers in the parentheses are the total number of tree-level observations, and circles are the mean values. The p-values were from the two-sample t-test with a null hypothesis that the group mean of 2012 is greater than that of 2013.

343 *Leaf-scale spectral indices*

344 Contrary to expectation, scaled PRI (*sPRI*) values of sunlit and shaded leaves did not show any
345 consistent patterns between dry and wet years (Figure 3), and the correlation analyses with the leaf PS
346 measurements did not show any significant results at tree and species levels. The sPRI values of the
347 sunlit leaves were generally lower compared to those of the shaded leaves in both years, which may
348 effectively represent higher LUE in shaded portion of canopy. The mean sPRI values of the sunlit
349 leaves (except for sassafras) were generally lower in 2012 (dry) than in 2013 (wet), while those of the
350 shaded leaves were generally higher in 2012 (except for tulip poplar) (Figure 3). The sPRI values
351 showed more interannual variability for the three isohydric species, while they were not significantly
352 different for two oak species (Figure 3d). These contrasting patterns between isohydric and
353 anisohydric species led to the difference in the sunlit-to-shaded PRI ratios between dry and wet years
354 (Figure 4). For all three isohydric species, the mean sPRI ratios ($sPRI_{sunlit}/sPRI_{shaded}$) were significantly
355 lower in 2012 ($p < 0.05$), while not for the two oak species ($p > 0.05$). This demonstrates that the
356 decreases in sPRI were much greater for sunlit than for shaded leaves during the drought, consistent
357 with the leaf-level PS measurements (Figure 3).

358 For the other spectral indices (NDVI, $NDVI_{705}$, and EVI), only EVI showed consistently and
359 statistically lower mean values in 2012 for both sunlit and shaded leaves, compared to 2013 (except
360 for the sunlit leaves of sassafras; Figure S5). $NDVI_{705}$ showed slightly better performance to capture
361 the drought effect and isohydric/anisohydric behavior than NDVI, but these patterns were still not
362 consistent. All three spectral indices did not show any distinct inter-annual differences between the
363 oak species and others, including their sunlit-to-shaded ratios (Figure S6). Thus all three of the
364 greenness spectral indices failed to capture isohydric vs. anisohydric behavior under the drought
365 condition, supporting that there is no clear evidence that drought-induced changes in leaf PS has any
366 direct implications on these three spectral indices.

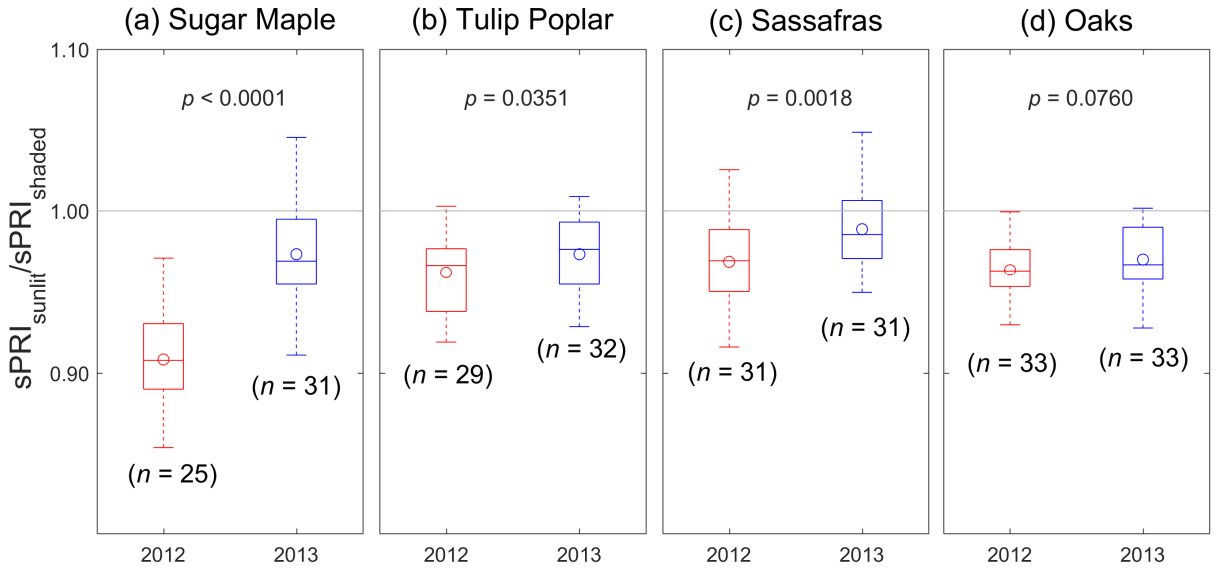

Figure 4: Boxplots for the sunlit-to-shaded sPRI ratios (dimensionless) from July to August in 2012 (drought year - red) and 2013 (wet year - blue) for three isohydric species: (a) sugar maple, (b) tulip poplar, (c) sassafras, and (d) anisohydric oak species (two white oaks and one red oak). All measurements represent the tree-level observations from three trees in each group, calculated from five sunlit and five shaded leaves from each tree. The numbers in the parentheses are the total number of tree-level observations, and circles show the mean values. The *p*-values were from the two-sample *t*-test with a null hypothesis that the group mean of 2012 is greater than that of 2013.

374 *Canopy-scale spectral indices*

375 The canopy-scale NDVI and EVI values showed clear differences between 2012 (dry) and 2013
376 (wet) years during the peak drought season (July-August) (Figure 5). Although both vegetation indices
377 show little interannual variability in their maximum values for the period from 2001 to 2014, the mean
378 NDVI and EVI values (July-August) were 5% and 11% less, respectively, in 2012 compared to the
379 mean for 2001-2014 (except 2012). Since leaf NDVI was largely unaffected by drought (Figure S5)
380 and the decrease in canopy NDVI roughly corresponded with the observed decrease in LAI values
381 (about 5-10 %) (Figure 5c), the changes in canopy structure appear to account for much of the change
382 in NDVI during the drought. On the other hand, canopy EVI declined slightly more during the drought
383 than did NDVI, indicating that both canopy structural and leaf spectral changes were factors in the
384 change in canopy EVI. However, note that decreases in both NDVI and EVI values were substantially
385 smaller than the changes in GEP and NEE values during the drought period (Figure 1).

386 Similar to the leaf-scale measurements, the pixel-level MODIS sPRI values during the peak
387 drought period (July-August) did not show consistent or statistically different patterns between dry
388 and wet years for both Terra and Aqua images (Figure 6). The MODIS sPRI values were generally
389 higher than the field observations, possibly due to the difference in the reference band. However, the
390 sPRI values from backward direction images were significantly lower than forward ones in 2012 for
391 both Terra and Aqua images ($p < 0.1$) (Figure 6). This demonstrates that the decreases in sPRI were
392 much greater in the sunlit portion of the canopy than in shaded portions during the peak drought,
393 consistent with the leaf-level spectral and PS measurements (Figure 3 and 4). As a result, the
394 backward-to-forward sPRI ratios were consistently lower during the peak drought period (July-August)
395 in 2012 than those in the normal and wet years (Figure 7). This was similar to the lower sunlit-to-
396 shade sPRI ratios at the leaf scale in 2012 (Figure 4), although the absolute ratio values are slightly
397 higher at the canopy scale. Given the <10% basal area composition of the anisohydric species in the
398 study site, it is possible that the leaf-level PRI signal of the isohydric species should be visible at the

399 MODIS pixel scale. However, note that the seasonal drought patterns were more obvious in the Aqua
400 data (local overpass time of approximately 1:30 PM; Figure 7b) than in Terra data (10:30 AM; Figure
401 7a), which more resemble GEP and NEE patterns in 2012 and 2013 (Figure 1). Additionally, these
402 ratios generally remained higher in 2013 (wet), compared to those at the same time in the other two
403 years.
404

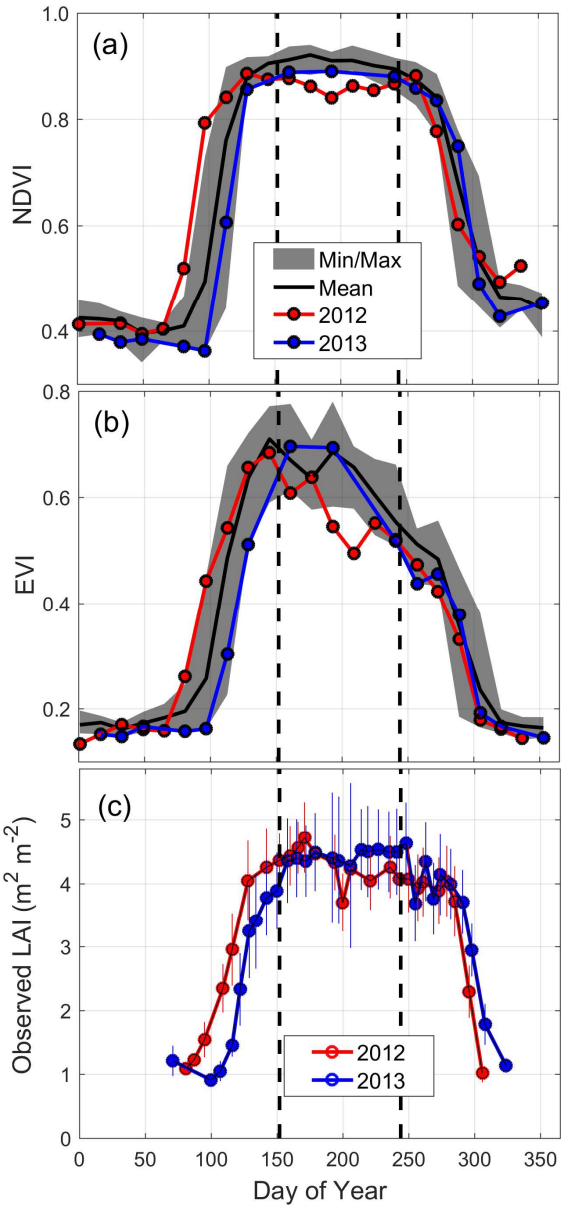

405

406 Figure 5: Seasonal patterns of MODIS (a) NDVI and (b) EVI (MOD13Q1), (c) observed LAI
407 (leaf are index) in 2012 (dry) and 2013 (wet) years. The gray regions represent the minimum
408 and maximum ranges of NDVI and EVI values from 2001 to 2015, except for 2012. LAI
409 values were measured weekly along the three transects around the flux tower (n = 30 total),
410 and the vertical lines represent the standard deviations. The vertical dashed lines show the
411 peak growing season (June-August) of the year.

412

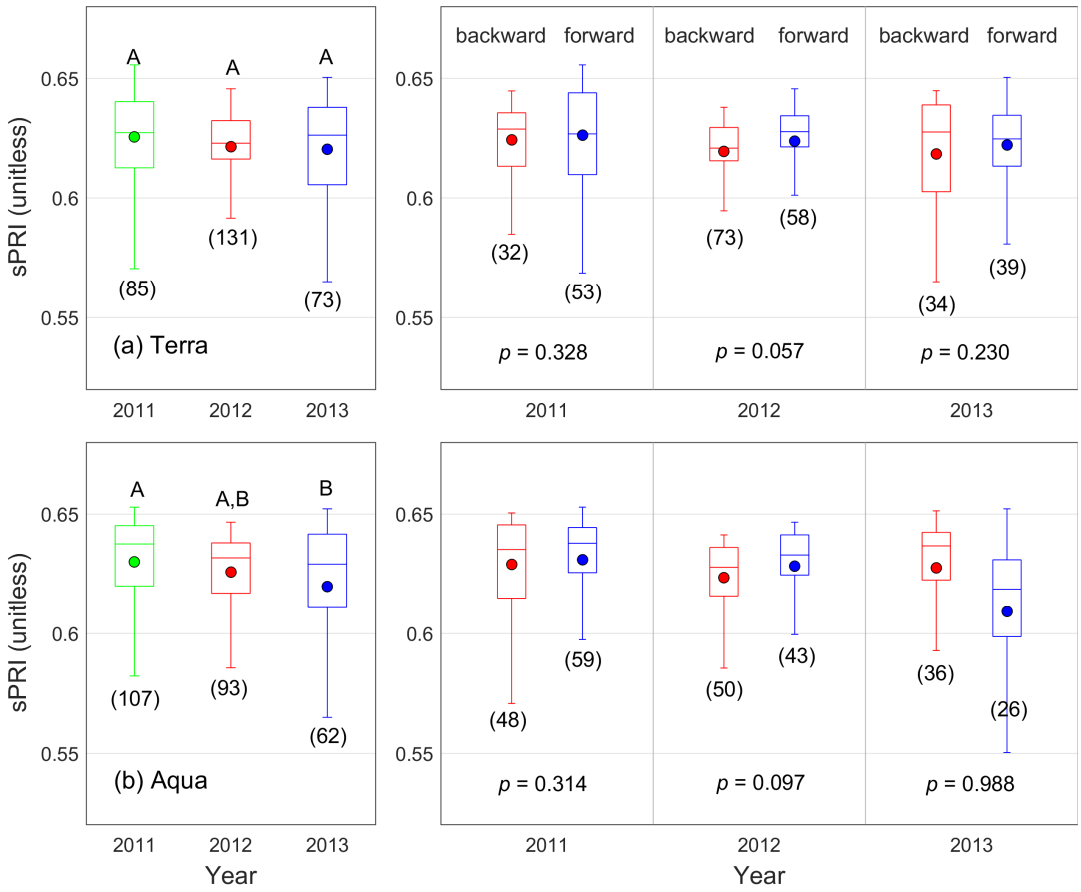

413

414 Figure 6: All sPRI values obtained from MODIS (a) Terra and (b) Aqua data from July
415 through August in normal (2011 – green), dry (2012 – red), and wet (2013 – blue) years. Bar
416 graphs in the right column show the pixel-level PRI values from the backward (red) and
417 forward (blue) direction MODIS images each year. Backward direction images include more
418 sunlit portion of the canopy, while forward direction images include more shaded portion. The
419 numbers in the parentheses are the total number of pixel-level MODIS PRI values used in
420 the study (Figure S7), and circles show the mean values. Different letters (A-B) denote
421 significant differences in the group means using an analysis of variance (ANOVA) test ($p <$
422 0.05). The *p*-values were from the two-sample *t*-test with a null hypothesis that the group
423 mean of 2012 is greater than that of 2013.

424

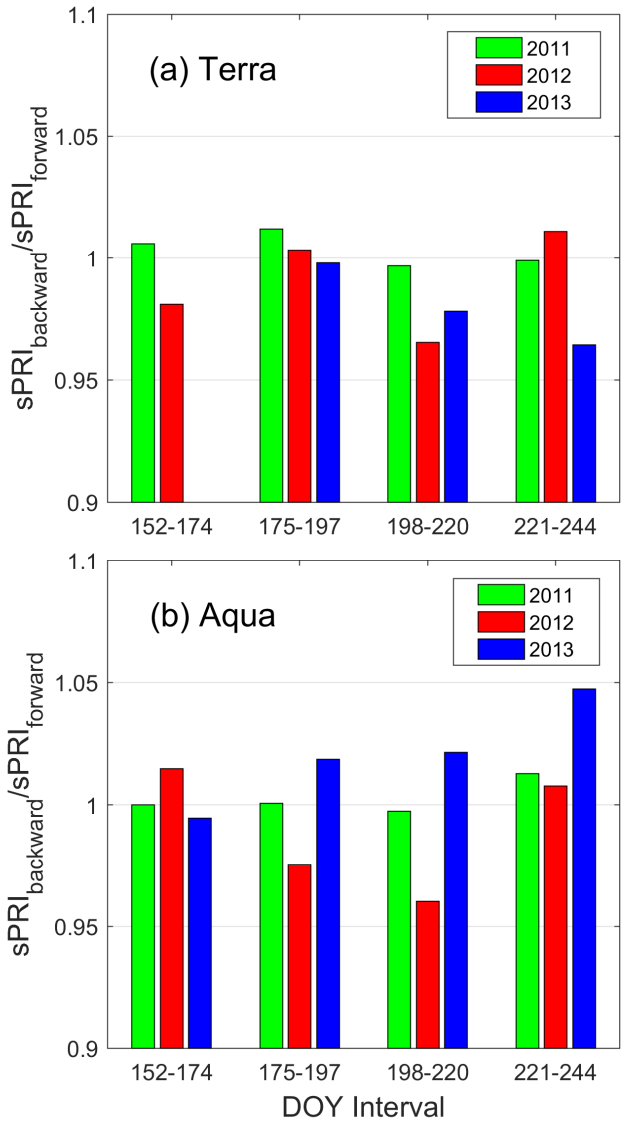

425

426 Figure 7: The sPRI ratios of backward to forward direction images for MODIS (a) Terra and
427 (b) Aqua data from June through August in normal (2011 – green), dry (2012 – red), and wet
428 (2013 – blue) years in the study site. The definition of backward and forward direction
429 MODIS images are provided in Eq. 3. The sPRI ratios were calculated roughly at three-week
430 intervals from the group means of the pixel-level MODIS PRI values at each day of year
431 (DOY) interval (Figure S7).

432

Discussion and conclusions

In this study, we examined the capability of four spectral indices to capture peak drought signals and isohydric/anisohydric behavior at both leaf and canopy scales in the closed deciduous broadleaf forest. NDVI and $NDVI_{705}$ failed to capture the drought signal or the divergent isohydric/anisohydric behavior at the leaf scale, while NDVI did show the canopy-scale structural changes (e.g. LAI) caused by the drought. EVI successfully captured the drought signals at both leaf and canopy scales, but failed to capture the isohydric/anisohydric behavior. Finally, PRI captured both drought signals and divergent isohydric/anisohydric behavior at both leaf and canopy scales once normalized between sunlit (backward direction) and shaded (forward direction) portions of canopy. Consistent with previous literature (e.g. Cheng et al. 2012; Hall et al. 2008), our results showed the directional responses of PRI were larger when drought stress and subsequent photosynthetic downregulation were greater in the sunlit portion of canopy. It is worthwhile to note that the seasonal drought signals in backward/forward PRI ratios from the MODIS Aqua data were more similar with GEP, NEE, and soil moisture patterns than those from Terra data.

Although PRI captures instantaneous energy dissipations in the xanthophyll cycle, it can be also influenced by seasonal and interannual changes including carotenoid-to-chlorophyll pigment ratios (Filella et al. 2009; Sims et al. 2006; Wong and Gamon 2015) and sun-target-sensor geometry (Gamon and Bond 2013). It is also well-known that trees retranslocate their leaf nitrogen under severe drought conditions (Heckathorn and DeLucia 1994), which might also affect the interannual LUE and PRI values between wet and dry years (Garbulsky et al. 2011). Therefore, seasonal and interannual variability of PRIs can be readily confounded by multiple environmental factors, which makes it difficult to detect and standardize drought stress using PRIs (Soudani et al. 2014; Zarco-Tejada et al. 2013; Zhang et al. 2016). Although there were the significant interannual changes in carbon uptakes both at the leaf and canopy scales, we also did not see any consistent shifts or apparent trends in the PRI values between wet and dry years. Likewise, we could not find any significant correlations

458 between the PRI values and the leaf PS measurements both at tree and species levels. However, once
459 normalized using sunlit-to-shade (leaf scale) and backward-to-forward image (canopy scale) ratios
460 under the assumption of increasing the degree of down-regulation during droughts, we could
461 successfully capture the drought effect on divergent behaviors between wet and dry years, between
462 isohydric and anisohydric tree species, and possibly between morning (Terra) and afternoon (Aqua)
463 MODIS images.

464 Our analysis also agrees well with a recent study by Vicca et al. (2016), who reported that only
465 EVI is capable of detecting drought signals at Hesse Forest in the northeastern France (also a
466 deciduous forest), while PRI and NDVI values did not capture the interannual changes in GPP caused
467 by drought. EVI was originally designed to reduce the spectral variances driven by atmospheric
468 aerosols by including the blue band (Huete et al. 2002). However, it is also sensitive to carotenoid
469 contents, which have high absorption between 400 and 500 nm (Sims and Gamon 2002) and usually
470 increases during droughts (Liu et al. 2011). However, EVI failed to capture divergent isohydric vs.
471 anisohydric behavior upon drought stress, clearly manifested in the leaf-level PS measurements.
472 Therefore, it is likely that the reduction of EVI during the drought period was driven not by emergent
473 differences in photosynthetic activities, but by the accompanying leaf physiological changes as well as
474 the structural changes at the canopy level, as suggested by Vicca et al. (2016).

475 Recently, two normalization methods for PRI were proposed by Zarco-Tejada et al. (2013) and
476 Soudani et al. (2014) at different time scales. Zarco-Tejada et al. (2013) used both renormalized
477 difference vegetation and red edge ratio indices to normalize PRI with the drought-induced changes in
478 chlorophyll content and vegetation structure at diurnal scale. Soudani et al. (2014) proposed the
479 correction of PRI values using intercepts of the linear regressions between APAR and PRI (called PRI_0)
480 at seasonal scale. Our normalization method intended to detect species-level responses to severe
481 droughts (isohydricity vs. anisohydricity) for closed deciduous forests, where traditional spectral
482 indices often have limited capability to capture drought-induced structural and/or chlorophyll-related

changes due to saturation problems (e.g. Daughtry et al. 2000). Additionally, we reported the divergence of PRI values between sunlit and shaded canopy portions consistently across leaf, canopy, and species levels, which would provide a unique advantage in upscaling drought effect on ecosystem carbon sequestration using spectral remote sensing information. However, the suggested method using backward and forward direction images may not be suitable for sparse forests. It is simply because this method explicitly assumes mutual shadowing between trees (viewing and illumination shadows on vegetative surfaces) are dominant factors controlling canopy bidirectional reflectance distribution function (BRDF) (Li and Strahler 1992; Li et al. 1995).

Although the divergence in MODIS PRI values between backward (sunlit) and forward (shaded) direction images were found in both Terra and Aqua data, the drought pattern in the sPRI ratios were more obvious in the Aqua data, compared to the Terra. There are two possible explanations for this. First, it might be mainly due to calibration issues of Terra by the problem in the solar diffuser door (e.g. Franz et al. 2008), which affects more the shorter wavelength bands. This issue was expected to be improved in the MODIS Collection 6, but it is quite possible that it did not completely remove the problems identified in the Collection 5 (Wu et al. 2013). Note that Gamon et al. (2016) also only used Aqua data to calculate CCI to monitor evergreen photosynthetic activity. Second, the drought stress and subsequent photosynthetic downregulation are likely to be greater in the afternoon rather than in the morning (Sims et al. 2005). The hourly LUE values from the flux tower also usually showed strong diurnal patterns especially in the non-cloudy days (Figure S8). These LUE values and their variances are often higher in the morning and lower in the afternoon, which might make drought signals unclear for the Terra data.

Many coupled modeling efforts have shown that separate modeling between sunlit and shaded portions of canopy was the most efficient way to simulate daily photosynthesis without multilayer simulations (Chen et al. 1999; de Pury and Farquhar 1997; Song et al. 2009; Wang and Leuning 1998). The dynamic separation between sunlit and shaded leaves is also justified in that the upper sunlit

508 canopy is usually light saturated (lower LUE), and therefore more vulnerable to drought stress, while
509 the lower shaded canopy responds linearly to irradiance with higher LUE (de Pury and Farquhar 1997;
510 Wang and Leuning 1998). This vertical transition of rate determining factors for photosynthesis
511 typically led to the distributions of leaf biochemical and structural traits along canopy depth profile,
512 such as carbon-to-nitrogen ratios and specific leaf area (Field, 1983; de Pury & Farquhar, 1997).
513 Recently, Coops et al. (2017) also showed that incorporating vertical gradients of PRI-derived LUE is
514 critical in upscaling leaf-scale physiological behavior into canopy-level GPP in the closed deciduous
515 canopy. However, to date few remote sensing based global GPP models incorporate two-leaf modeling
516 structures because of computational efficiency (Zhou et al. 2015). In this study, we suggest that it
517 would be critical to incorporate the two-leaf model structure to properly simulate the drought effect on
518 ecosystem carbon sequestrations under climate change considering emergent divergence between
519 sunlit and shade portions of canopy.
520 Parameterizing water use strategies into terrestrial ecosystem models will essentially require
521 mapping the distribution of anisohydric and isohydric trees across the different spatial scales. However,
522 mapping isohydricity from the parameter space along the isohydric/anisohydric continuum to
523 landscape space requires very detailed vegetation information with intensive field observations during
524 drought (Meinzer et al. 2016). To date, we are aware of only one attempt to develop a map of the
525 distribution of isohydricity across the landscape (Konings and Gentine 2016). That work relied on
526 remotely-sensed observations of vegetation optical depth using Advanced Microwave Scanning
527 Radiometer-E (AMSR-E) data, which has been previously shown to be correlated with leaf water
528 potential. Our approach suggests another path forward for using emergent spectral signatures during
529 droughts to map the distribution of isohydric and anisohydric species. This study presents a theoretical
530 framework for large-scale isohydricity mapping based on emergent spectral signatures under drought
531 stress using multi-angle MODIS images. This direct mapping of ecosystem sensitivity to drought
532 stress may represent a significant step forward from the simplistic drought scalars currently used in

533 remote-sensing based productivity models.

534

535 *Conclusions*

536 In this study, we examined the capability of four spectral indices to capture peak drought signals
537 and isohydric/anisohydric behavior in a deciduous broadleaf forest using in-situ spectral
538 measurements and multi-angle remote sensing images. After normalizing between sunlit (backward)
539 and shaded (forward) portions of canopy, PRI successfully captured both drought signals and species-
540 level drought responses at both leaf and canopy scales. Drought stress and subsequent photosynthetic
541 downregulation were greater in the sunlit portion of canopy, which provides us a key to capture
542 species- and canopy-level drought responses in the study site. Importantly, this work may represent a
543 significant step forward in our ability to dynamically predict the impact of water stress on forest
544 carbon gain by providing a theoretical framework for mapping large-scale isohydricity based on
545 emergent spectral responses under drought stress.

546

547 **Acknowledgements**

548 This research was supported by NASA Carbon Science program (Grant # NNX17AE69G) to Drs.
549 T Hwang and K Novick. Funding for the leaf-scale PS and spectral measurements was provided by the
550 NASA Terrestrial Ecology program (Grant # NNX10AF40G) to Drs. A.F. Rahman and D.A. Sims.
551 Funding for the Morgan Monroe Flux Tower is provided by the AmeriFlux Management Project,
552 administered by Lawrence Berkeley National Lab with support from the US Department of Energy.
553 We thanks to three anonymous reviewers for their constructive comments and supports. We also thank
554 to Steve Scott, Bo Stearman, and Rob Conover for help in collection of field data.

555

References

Adams, H.D., Guardiola-Claramonte, M., Barron-Gafford, G.A., Villegas, J.C., Breshears, D.D., Zou, C.B., Troch, P.A., & Huxman, T.E. (2009). Temperature sensitivity of drought-induced tree mortality portends increased regional die-off under global-change-type drought. *Proceedings of the national academy of sciences, 106*, 7063-7066

Allen, C.D., & Breshears, D.D. (2007). Climate-induced forest dieback as an emergent global phenomenon. *Eos, Transactions American Geophysical Union, 88*, 504-504

Asner, G.P., Nepstad, D., Cardinot, G., & Ray, D. (2004). Drought stress and carbon uptake in an Amazon forest measured with spaceborne imaging spectroscopy. *Proc Natl Acad Sci U S A, 101*, 6039-6044

Barton, C.V.M., & North, P. (2001). Remote sensing of canopy light use efficiency using the photochemical reflectance index: Model and sensitivity analysis. *Remote Sensing of Environment, 78*, 264-273

Brzostek, E.R., Dragoni, D., Schmid, H.P., Rahman, A.F., Sims, D., Wayson, C.A., Johnson, D.J., & Phillips, R.P. (2014). Chronic water stress reduces tree growth and the carbon sink of deciduous hardwood forests. *Glob Chang Biol, 20*, 2531-2539

Chen, J.M., Liu, J., Cihlar, J., & Goulden, M.L. (1999). Daily canopy photosynthesis model through temporal and spatial scaling for remote sensing applications. *Ecological Modelling, 124*, 99-119

Cheng, Y.-B., Middleton, E.M., Zhang, Q., Corp, L.A., Dandois, J., & Kustas, W.P. (2012). The photochemical reflectance index from directional cornfield reflectances: observations and simulations. *Remote Sensing of Environment, 124*, 444-453

Choat, B., Jansen, S., Brodribb, T.J., Cochard, H., Delzon, S., Bhaskar, R., Bucci, S.J., Feild, T.S., Gleason, S.M., Hacke, U.G., Jacobsen, A.L., Lens, F., Maherali, H., Martinez-Vilalta, J., Mayr, S., Mencuccini, M., Mitchell, P.J., Nardini, A., Pittermann, J., Pratt, R.B., Sperry, J.S., Westoby, M., Wright, I.J., & Zanne, A.E. (2012). Global convergence in the vulnerability of forests to drought. *Nature, 491*, 752-755

Coops, N.C., Hermosilla, T., Hilker, T., & Black, T.A. (2017). Linking stand architecture with canopy reflectance to estimate vertical patterns of light-use efficiency. *Remote Sensing of Environment, 194*, 322-330

Coops, N.C., Hilker, T., Hall, F.G., Nichol, C.J., & Drolet, G.G. (2010). Estimation of light-use efficiency of terrestrial ecosystems from space: a status report. *BioScience, 60*, 788-797

Dai, A. (2013). Increasing drought under global warming in observations and models. *Nature Climate Change, 3*, 52-58

Daughtry, C., Walthall, C., Kim, M., De Colstoun, E.B., & McMurtrey, J. (2000). Estimating corn leaf chlorophyll concentration from leaf and canopy reflectance. *Remote Sensing of Environment, 74*, 229-239

de Pury, D.G.G., & Farquhar, G.D. (1997). Simple scaling of photosynthesis from leaves to canopies without the errors of big-leaf models. *Plant Cell and Environment, 20*, 537-557

Demmig-Adams, B., & Adams III, W.W. (1996). Xanthophyll cycle and light stress in nature: uniform response to excess direct sunlight among higher plant species. *Planta, 198*, 460-470

Didan, K., & Huete, A. (2006). MODIS Vegetation Index Product Series Collection 5 Change

598 Summary. In: TBRS Lab., University of Arizona

599 Dragoni, D., Schmid, H.P., Wayson, C.A., Potter, H., Grimmond, C.S.B., & Randolph, J.C.
600 (2011). Evidence of increased net ecosystem productivity associated with a longer vegetated
601 season in a deciduous forest in south-central Indiana, USA. *Global Change Biology, 17*, 886-
602 897

603 Drolet, G., Middleton, E., Huemmrich, K., Hall, F., Amiro, B., Barr, A., Black, T., McCaughey,
604 J., & Margolis, H. (2008). Regional mapping of gross light-use efficiency using MODIS
605 spectral indices. *Remote Sensing of Environment, 112*, 3064-3078

606 Drolet, G.G., Huemmrich, K.F., Hall, F.G., Middleton, E.M., Black, T.A., Barr, A.G., &
607 Margolis, H.A. (2005). A MODIS-derived photochemical reflectance index to detect inter-
608 annual variations in the photosynthetic light-use efficiency of a boreal deciduous forest.
609 *Remote Sensing of Environment, 98*, 212-224

610 Ehman, J., Schmid, H., Grimmond, C., Randolph, J., Hanson, P., Wayson, C., & Cropley, F.
611 (2002). An initial intercomparison of micrometeorological and ecological inventory estimates
612 of carbon exchange in a mid-latitude deciduous forest. *Global change biology, 8*, 575-589

613 Filella, I., Porcar-Castell, A., Munné-Bosch, S., Bäck, J., Garbulsky, M.F., & Peñuelas, J.
614 (2009). PRI assessment of long-term changes in carotenoids/chlorophyll ratio and short-term
615 changes in de-epoxidation state of the xanthophyll cycle. *International Journal of Remote*
616 *Sensing, 30*, 4443-4455

617 Ford, C.R., Hubbard, R.M., & Vose, J.M. (2011). Quantifying structural and physiological
618 controls on variation in canopy transpiration among planted pine and hardwood species in
619 the southern Appalachians. *Ecohydrology, 4*, 183-195

620 Franz, B.A., Kwiatowska, E.J., Meister, G., & McClain, C.R. (2008). Moderate Resolution
621 Imaging Spectroradiometer on Terra: limitations for ocean color applications. *Journal of*
622 *Applied Remote Sensing, 2*, 023525

623 Gamon, J., Penuelas, J., & Field, C. (1992). A narrow-waveband spectral index that tracks
624 diurnal changes in photosynthetic efficiency. *Remote Sensing of Environment, 41*, 35-44

625 Gamon, J., Serrano, L., & Surfus, J. (1997). The photochemical reflectance index: an optical
626 indicator of photosynthetic radiation use efficiency across species, functional types, and
627 nutrient levels. *Oecologia, 112*, 492-501

628 Gamon, J.A., & Bond, B. (2013). Effects of irradiance and photosynthetic downregulation on
629 the photochemical reflectance index in Douglas-fir and ponderosa pine. *Remote Sensing of*
630 *Environment, 135*, 141-149

631 Gamon, J.A., Huemmrich, K.F., Wong, C.Y., Ensminger, I., Garrity, S., Hollinger, D.Y.,
632 Noormets, A., & Penuelas, J. (2016). A remotely sensed pigment index reveals
633 photosynthetic phenology in evergreen conifers. *Proc Natl Acad Sci U S A*

634 Garbulsky, M.F., Peñuelas, J., Gamon, J., Inoue, Y., & Filella, I. (2011). The photochemical
635 reflectance index (PRI) and the remote sensing of leaf, canopy and ecosystem radiation use
636 efficiencies: a review and meta-analysis. *Remote Sensing of Environment, 115*, 281-297

637 Garbulsky, M.F., Peñuelas, J., Ogaya, R., & Filella, I. (2013). Leaf and stand-level carbon
638 uptake of a Mediterranean forest estimated using the satellite-derived reflectance indices EVI
639 and PRI. *International journal of remote sensing, 34*, 1282-1296

640 Goerner, A., Reichstein, M., & Rambal, S. (2009). Tracking seasonal drought effects on
641 ecosystem light use efficiency with satellite-based PRI in a Mediterranean forest. *Remote*

sensing of environment, 113, 1101-1111

Goerner, A., Reichstein, M., Tomelleri, E., Hanan, N., Rambal, S., Papale, D., Dragoni, D., & Schmullius, C. (2011). Remote sensing of ecosystem light use efficiency with MODIS-based PRI. *Biogeosciences, 8*, 189-202

Hall, F.G., Hilker, T., & Coops, N.C. (2012). Data assimilation of photosynthetic light-use efficiency using multi-angular satellite data: I. Model formulation. *Remote Sensing of Environment, 121*, 301-308

Hall, F.G., Hilker, T., Coops, N.C., Lyapustin, A., Huemmrich, K.F., Middleton, E., Margolis, H., Drolet, G., & Black, T.A. (2008). Multi-angle remote sensing of forest light use efficiency by observing PRI variation with canopy shadow fraction. *Remote Sensing of Environment, 112*, 3201-3211

He, M., Kimball, J.S., Running, S., Ballantyne, A., Guan, K., & Huemmrich, F. (2016). Satellite detection of soil moisture related water stress impacts on ecosystem productivity using the MODIS-based photochemical reflectance index. *Remote Sensing of Environment, 186*, 173-183

Heckathorn, S.A., & DeLucia, E.H. (1994). Drought-induced nitrogen retranslocation in perennial C4 grasses of tallgrass prairie. *Ecology, 75*, 1877-1886

Hilker, T., Coops, N.C., Hall, F.G., Black, T.A., Wulder, M.A., Nesic, Z., & Krishnan, P. (2008). Separating physiologically and directionally induced changes in PRI using BRDF models. *Remote Sensing of Environment, 112*, 2777-2788

Huete, A.R., Liu, H.Q., Batchily, K., & vanLeeuwen, W. (1997). A comparison of vegetation indices global set of TM images for EOS-MODIS. *Remote Sensing of Environment, 59*, 440-451

Hwang, T., Kang, S., Kim, J., Kim, Y., Lee, D., & Band, L. (2008). Evaluating drought effect on MODIS Gross Primary Production (GPP) with an eco-hydrological model in the mountainous forest, East Asia. *Global Change Biology, 14*, 1037-1056

Klein, T., Yakir, D., Buchmann, N., & Gruenzweig, J.M. (2014). Towards an advanced assessment of the hydrological vulnerability of forests to climate change-induced drought. *New Phytologist, 201*, 712-716

Konings, A.G., & Gentine, P. (2016). Global variations in ecosystem-scale isohydricity. *Global Change Biology*

Li, X., & Strahler, A.H. (1992). Geometric-optical bidirectional reflectance modeling of the discrete crown vegetation canopy: Effect of crown shape and mutual shadowing. *IEEE Transactions on Geoscience and Remote Sensing, 30*, 276-292

Li, X., Strahler, A.H., & Woodcock, C.E. (1995). A hybrid geometric optical-radiative transfer approach for modeling albedo and directional reflectance of discontinuous canopies. *IEEE Transactions on Geoscience and Remote Sensing, 33*, 466-480

Liu, C., Liu, Y., Guo, K., Fan, D., Li, G., Zheng, Y., Yu, L., & Yang, R. (2011). Effect of drought on pigments, osmotic adjustment and antioxidant enzymes in six woody plant species in karst habitats of southwestern China. *Environmental and Experimental Botany, 71*, 174-183

Marchin, R., Zeng, H., & Hoffmann, W. (2010). Drought-deciduous behavior reduces nutrient losses from temperate deciduous trees under severe drought. *Oecologia, 163*, 845-854

685 Martinez-Vilalta, J., Poyatos, R., Aguade, D., Retana, J., & Mencuccini, M. (2014). A new
686 look at water transport regulation in plants. *New Phytologist, 204*, 105-115

687 Matheny, A.M., Fiorella, R.P., Bohrer, G., Poulsen, C.J., Morin, T.H., Wunderlich, A., Vogel,
688 C.S., & Curtis, P.S. (2016). Contrasting strategies of hydraulic control in two codominant
689 temperate tree species. *Ecohydrology*

690 McDowell, N., Pockman, W.T., Allen, C.D., Breshears, D.D., Cobb, N., Kolb, T., Plaut, J.,
691 Sperry, J., West, A., Williams, D.G., & Yepez, E.A. (2008). Mechanisms of plant survival and
692 mortality during drought: why do some plants survive while others succumb to drought? *New*
693 *Phytologist, 178*, 719-739

694 McDowell, N.G., & Allen, C.D. (2015). Darcy's law predicts widespread forest mortality under
695 climate warming. *Nature Climate Change, 5*, 669-672

696 Meinzer, F.C., Smith, D.D., Woodruff, D.R., Marias, D.E., McCulloh, K.A., Howard, A.R., &
697 Magedman, A.L. (2017). Stomatal kinetics and photosynthetic gas exchange along a
698 continuum of iso-to anisohydric regulation of plant water status. *Plant, cell & environment*

699 Meinzer, F.C., Woodruff, D.R., Marias, D.E., Smith, D.D., McCulloh, K.A., Howard, A.R., &
700 Magedman, A.L. (2016). Mapping 'hydroscapes' along the iso- to anisohydric continuum of
701 stomatal regulation of plant water status. *Ecol Lett, 19*, 1343-1352

702 Munne-Bosch, S., Jubany-Mari, T., & Alegre, L. (2001). Drought-induced senescence is
703 characterized by a loss of antioxidant defences in chloroplasts. *Plant Cell and Environment,*
704 *24*, 1319-1327

705 Novick, K.A., Miniat, C.F., & Vose, J.M. (2016). Drought limitations to leaf-level gas
706 exchange: results from a model linking stomatal optimization and cohesion-tension theory.
707 *Plant Cell Environ, 39*, 583-596

708 Novick, K.A., Oishi, A.C., Ward, E.J., Siqueira, M.B., Juang, J.Y., & Stoy, P.C. (2015). On the
709 difference in the net ecosystem exchange of CO2 between deciduous and evergreen forests
710 in the southeastern United States. *Glob Chang Biol, 21*, 827-842

711 Penuelas, J., Filella, I., & Gamon, J.A. (1995). Assessment of photosynthetic radiation-use
712 efficiency with spectral reflectance. *New Phytologist, 131*, 291-296

713 Rahman, A., Cordova, V., Gamon, J., Schmid, H., & Sims, D. (2004). Potential of MODIS
714 ocean bands for estimating CO2 flux from terrestrial vegetation: A novel approach.
715 *Geophysical Research Letters, 31*

716 Roman, D., Novick, K., Brzostek, E., Dragoni, D., Rahman, F., & Phillips, R. (2015). The role
717 of isohydric and anisohydric species in determining ecosystem-scale response to severe
718 drought. *Oecologia, 179*, 641-654

719 Schmid, H.P., Grimmond, C.S.B., Cropley, F., Offerle, B., & Su, H.-B. (2000). Measurements
720 of CO 2 and energy fluxes over a mixed hardwood forest in the mid-western United States.
721 *Agricultural and Forest Meteorology, 103*, 357-374

722 Sims, D.A., Brzostek, E.R., Rahman, A.F., Dragoni, D., & Phillips, R.P. (2014). An improved
723 approach for remotely sensing water stress impacts on forest C uptake. *Global Change*
724 *Biology, 20*, 2856-2866

725 Sims, D.A., & Gamon, J.A. (2002). Relationships between leaf pigment content and spectral
726 reflectance across a wide range of species, leaf structures and developmental stages.
727 *Remote Sensing of Environment, 81*, 337-354

728 Sims, D.A., Luo, H., Hastings, S., Oechel, W.C., Rahman, A.F., & Gamon, J.A. (2006).
729 Parallel adjustments in vegetation greenness and ecosystem CO 2 exchange in response to
730 drought in a Southern California chaparral ecosystem. *Remote Sensing of Environment, 103*,
731 289-303

732 Sims, D.A., Rahman, A.F., Cordova, V.D., Baldocchi, D.D., Flanagan, L.B., Goldstein, A.H.,
733 Hollinger, D.Y., Misson, L., Monson, R.K., & Schmid, H.P. (2005). Midday values of gross
734 CO2 flux and light use efficiency during satellite overpasses can be used to directly estimate
735 eight-day mean flux. *Agricultural and Forest Meteorology, 131*, 1-12

736 Song, C., Dannenberg, M.P., & Hwang, T. (2013). Optical remote sensing of terrestrial
737 ecosystem primary productivity. *Progress in Physical Geography, 37*, 834-854

738 Song, C.H., Katul, G., Oren, R., Band, L.E., Tague, C.L., Stoy, P.C., & McCarthy, H.R.
739 (2009). Energy, water, and carbon fluxes in a loblolly pine stand: Results from uniform and
740 gappy canopy models with comparisons to eddy flux data. *Journal of Geophysical Research-*
741 *Biogeosciences, 114*, G04021

742 Soudani, K., Hmimina, G., Dufrêne, E., Berveiller, D., Delpierre, N., Ourcival, J.-M., Rambal,
743 S., & Joffre, R. (2014). Relationships between photochemical reflectance index and light-use
744 efficiency in deciduous and evergreen broadleaf forests. *Remote Sensing of Environment,*
745 *144*, 73-84

746 Sperry, J.S., Wang, Y., Wolfe, B.T., Mackay, D.S., Anderegg, W.R., McDowell, N.G., &
747 Pockman, W.T. (2016). Pragmatic hydraulic theory predicts stomatal responses to climatic
748 water deficits. *New Phytologist, 212*, 577-589

749 Stoy, P.C., Katul, G.G., Siqueira, M.B.S., Juang, J.-Y., Novick, K.A., McCarthy, H.R., Oishi,
750 A.C., Uebelherr, J.M., Kim, H.-S., & Oren, R. (2006). Separating the effects of climate and
751 vegetation on evapotranspiration along a successional chronosequence in the southeastern
752 US. *Global Change Biology, 12*, 2115-2135

753 Suárez, L., Zarco-Tejada, P.J., Sepulcre-Cantó, G., Pérez-Priego, O., Miller, J.R., Jiménez-
754 Muñoz, J., & Sobrino, J. (2008). Assessing canopy PRI for water stress detection with diurnal
755 airborne imagery. *Remote Sensing of Environment, 112*, 560-575

756 Sulman, B.N., Roman, D.T., Scanlon, T.M., Wang, L., & Novick, K.A. (2016). Comparing
757 methods for partitioning a decade of carbon dioxide and water vapor fluxes in a temperate
758 forest. *Agricultural and Forest Meteorology, 226*, 229-245

759 Tucker, C.J. (1979). Red and Photographic Infrared Linear Combinations for Monitoring
760 Vegetation. *Remote Sensing of Environment, 8*, 127-150

761 Vicca, S., Balzarolo, M., Filella, I., Granier, A., Herbst, M., Knohl, A., Longdoz, B., Mund, M.,
762 Nagy, Z., & Pintér, K. (2016). Remotely-sensed detection of effects of extreme droughts on
763 gross primary production. *Scientific Reports, 6*

764 Wang, Y.-P., & Leuning, R. (1998). A two-leaf model for canopy conductance,
765 photosynthesis and partitioning of available energy I:: Model description and comparison with
766 a multi-layered model. *Agricultural and Forest Meteorology, 91*, 89-111

767 Wong, C.Y., & Gamon, J.A. (2015). Three causes of variation in the photochemical
768 reflectance index (PRI) in evergreen conifers. *New Phytol, 206*, 187-195

769 Wu, A., Xiong, X., Doelling, D.R., Morstad, D., Angal, A., & Bhatt, R. (2013). Characterization
770 of Terra and Aqua MODIS VIS, NIR, and SWIR spectral bands' calibration stability. *IEEE*
771 *Transactions on Geoscience and Remote Sensing, 51*, 4330-4338

772 Xu, L., & Baldocchi, D.D. (2003). Seasonal trends in photosynthetic parameters and stomatal
773 conductance of blue oak (Quercus douglasii) under prolonged summer drought and high
774 temperature. *Tree Physiology, 23*, 865-877

775 Yi, K., Dragoni, D., Phillips, R.P., Roman, D.T., & Novick, K.A. (2017). Dynamics of stem
776 water uptake among isohydric and anisohydric species experiencing a severe drought. *Tree*
777 *Physiology*, 1-14

778 Zarco-Tejada, P.J., González-Dugo, V., Williams, L.E., Suárez, L., Berni, J.A.J., Goldhamer,
779 D., & Fereres, E. (2013). A PRI-based water stress index combining structural and
780 chlorophyll effects: Assessment using diurnal narrow-band airborne imagery and the CWSI
781 thermal index. *Remote Sensing of Environment, 138*, 38-50

782 Zhang, C., Filella, I., Garbulsky, M., & Peñuelas, J. (2016). Affecting Factors and Recent
783 Improvements of the Photochemical Reflectance Index (PRI) for Remotely Sensing Foliar,
784 Canopy and Ecosystemic Radiation-Use Efficiencies. *Remote Sensing, 8*, 677

785 Zhao, M., Heinsch, F.A., Nemani, R.R., & Running, S.W. (2005). Improvements of the
786 MODIS terrestrial gross and net primary production global data set. *Remote Sensing of*
787 *Environment, 95*, 164-176

788 Zhou, Y., Wu, X., Ju, W., Chen, J.M., Wang, S., Wang, H., Yuan, W., Black, A., Jassal, R., &
789 Ibrom, A. (2015). Global parameterization and validation of a two-leaf light use efficiency
790 model for predicting gross primary production across FLUXNET sites. *Journal of Geophysical*
791 *Research: Biogeosciences*

792